1-1-2011

First-Principles Study of the Site Occupancy and Magnetic Properties of Zinc-Tin-Substituted Strontium Hexaferrite

Serkan Guldal

FIRST-PRINCIPLES STUDY OF THE SITE OCCUPANCY AND MAGNETIC PROPERTIES OF ZINC-TIN-SUBSTITUTED STRONTIUM HEXAFERRITE

By

Serkan Guldal (Serkan Güldal)

A Thesis
Submitted to the Faculty of
Mississippi State University
in Partial Fulfillment of the Requirements
for the Degree of Master of Science
in Physics
in the Department of Physics and Astronomy

Mississippi State, Mississippi

August 2011

FIRST-PRINCIPLES STUDY OF THE SITE OCCUPANCY AND MAGNETIC PROPERTIES OF ZINC-TIN-SUBSTITUTED STRONTIUM HEXAFERRITE

By

Serkan Guldal (Serkan Güldal)

Approved:

Seong-Gon Kim Associate Professor of Physics (Major Professor)	David L. Monts Professor of Physics (Committee Member)
Matthew J. Berg Assistant Professor of Physics (Committee Member)	Mark A. Novotny Professor of Physics Department Head (Graduate Coordinator)

Gary L. Myers
Professor and Dean
College of Arts & Sciences

Name: Serkan Guldal (Serkan Güldal)

Date of Degree: August 6, 2011

Institution: Mississippi State University

Major Field: Physics

Major Professor: Dr. Seong-Gon Kim

Title of Study: FIRST-PRINCIPLES STUDY OF THE SITE OCCUPANCY AND MAGNETIC PROPERTIES OF ZINC-TIN-SUBSTITUTED STRONTIUM HEXAFERRITE

Pages in Study: 26

Candidate for Degree of Master of Science

I performed first principles studies of the site occupancy and magnetic properties of zinc-tin-substituted strontium hexaferrite by using density functional theory. In this study, I determined the site preference of zinc and tin atoms when they are restricted to occupy the same sublattice in strontium-hexaferrite. I found that Zn and Sn atoms prefer to replace Fe ions at $2a$ sublattice under this restriction and caused the saturation magnetization to decrease.

Key words: DFT, strontium hexaferrite, magnetic materials

DEDICATION

To My Family.

ACKNOWLEDGMENTS

This research project would not have been possible without the support of many people.

First, I wish to express my gratitude to my mentor Prof. Seong-Gon Kim for guiding me to complete this project.

I would also wish to give special thanks to all my graduate students friends. I am especially thankful to Laalitha Liyanage who helped me to become more familiar with the Linux operating system and the VASP simulation code. Moreover, his sharing of the literature and invaluable assistance is unforgettable.

I would like to extend my gratitude to Dr. David L. Monts, who was abundantly helpful and offered invaluable assistance. His guidance and advice were vital towards my graduation.

I would also like thank to Dr. Mark A. Novotny and Dr. Matthew J. Berg for their generosity in making themselves available for consultation and for their comments and suggestions on this thesis.

Also, I wish to thank my sponsor, the Republic of Turkey Ministry of National Education. I would like to convey thanks to the High Performance Computing Collaboratory (HPC2) for providing computing facilities.

Finally, I am thankful to my parents, Fikret Güldal, and Necla Güldal, my lovely sisters, Sümeyra Güldal, Suna Kaplan, and Seda Şeker, my only niece Pınar Yerce, and my nephews Ahmet Tamer Yerce, Muhammed Kubilah Kaplan, and Siraç Toprak Şeker, for motivating me to become a nice, hard working person rather than only a physicist.

TABLE OF CONTENTS

LIST OF TABLES

LIST OF FIGURES

CHAPTER 1

INTRODUCTION

Recently, computational sciences have been used in more areas. Computational methods are helpful for gaining results; scientists have to spend enormous amounts of money and time when they perform experiments. For instance, *ab initio* methods can produce results even when experimental results do not exist or are extremely difficult to obtain, or the experimental systems are unreliable. Most material properties depend on the interactions among electrons. Density functional theory (DFT) yields good results because DFT's results match well with experimental observations of structure and magnetic properties [31]. However, DFT has limitations, including the size of the systems that can be investigated and the amount of time each step requires. DFT is useful for finding the minimum energy structure of molecules.

The Schrödinger equation $\hat{H}\Psi = E\Psi$ can be solved for many-particle systems by using the electronic structure calculations. When a system with N particles evolves in three-dimensional space, $\hat{H}$ represents the Hamiltonian operator for the 3×N-dimensional wave function Ψ and E is the total energy of the system. Solving the Schrödinger equation exactly is not feasible for anything other than the hydrogen atom (one proton and one electron) in analytical form. On the other hand, the Hohenberg-Kohn theorem and DFT help to produce good results with reasonable

approximations for many-particle systems. DFT expresses the total energies of a functional instead of dealing with 3×N-dimensional wave functions, in which N is the number of electrons for three dimensional electron density calculations. Therefore, DFT is used to determine approximately the effective energy using an equivalent electron density. It is well established that minimizing the density functional produces reliable ground state density, so DFT can determine all properties of molecular systems, in the same manner as like a full wave function would [16]. Functionals, such as the generalized gradient approximation for the exchange-correlation (XC) energy functional, help to obtain more accurate results than local density approximations.

Valence electrons dominate the magnetic properties of materials. These electrons interact strongly with those of neighboring atoms. On the other hand, core electrons have weak interactions with neighboring atoms, being tightly bound to the nuclei. Therefore, alkali metals which have one valence electron are highly reactive. On the other hand, noble gases (such as He, Ne, Ar, etc.) have full shells containing 2, 8, or 18 electrons filling s, p, or d orbitals, respectively leaving no valence electrons, are chemically inert resulting in low solidification points.

Pseudopotentials are used for more efficient numerical computations. I used pseudopotentials in ultrasoft pseudopotential (USPP) or projector-augmented wave (PAW) formats to describe the interactions between ions and electrons [20, 3]. The exchange-correlation energy functional can be described both in formats local density approximation (LDA) or generalized gradient approximation (GGA) [36, 38].

Strontium hexaferrite ($SrO_{19}Fe_{12}$) is a permanent magnetic material. Due to its high saturation magnetization, good chemical stability, and large magneto-crystaline anisotropy, this material has been investigated intensively [34, 1]. The magnetic Fe^{3+} ions in the compound are arranged in five different sublattices. The three sublattices of ferric ions' spins in the $12k$, $2a$ and $2b$ sites are anti-parallel to those of the other ensemble ferrite ions in $4f_1$ and $4f_2$ sites. It has been found experimentally that the incorporation of tin (Sn) and zinc (Zn) in strontium hexaferrite increases the saturation magnetization and reduces magnetic anisotropy. Based on these results and Mössbauer spectroscopy measurements, Ghasemi et al. suggested that Zn and Sn atoms prefer $2b$ and $4f_2$ sites [12].

CHAPTER 2

DENSITY FUNCTIONAL THEORY

2.1 Introduction

Based on advances in computing power, many scientists have used DFT to understand physical systems, such as the properties of atoms, molecules, gases, and solid state matter. DFT is limited with regards to the maximum number of atoms, but periodic boundary conditions allow us to investigate properties of some bulk-like materials. Kohn established that the electron density functional can be used to describe the properties of systems [35]. Instead of solving the Schrödinger equation, DFT solves for the electron density n. This theory reduces many-body interactions to one effective-electron-equation which depends on the electron density. In this chapter, I will present the basic assumptions and methods used in DFT simulations.

2.1.1 Born-Oppenheimer Approximation

When the wave function is solved, the nuclei are considered fixed in place in a static potential field because the nuclei are much more massive than the electron. $\Psi(\mathrm{R}_1...\mathrm{R}_M;\mathrm{r}_1....\mathrm{r}_N)$ is the ground state wave function for a stationary state of a system with M nuclei at positions $\mathrm{R}_1....\mathrm{R}_M$ and N electrons at positions $\mathrm{r}_1...\mathrm{r}_N$ ob-

tained by solving the time-independent Schrödinger equation: $\hat{H}\psi(\mathrm{R}_1...\mathrm{R}_M;\mathrm{r}_1...\mathrm{r}_N)=E\psi(\mathrm{R}_1...\mathrm{R}_M;\mathrm{r}_1....\mathrm{r}_N)$. $\hat{H}$ is Hamiltonian operator:

$$\hat{H} = -\sum_{i=1}^{M}\frac{h^2}{2m_{Z_i}}\nabla^2_{R_i} - \sum_{i=1}^{N}\frac{h^2}{2m_e}\nabla^2_{r_i} + \frac{1}{4\pi\epsilon_0}\sum_{i=1}^{M}\sum_{j>i}^{M}\frac{Z_i Z_j e^2}{|R_i - R_j|} - \frac{1}{4\pi\epsilon_0}\sum_{i=1}^{N}\sum_{j=1}^{M}\frac{Z_j e^2}{|r_i - R_j|} + \frac{1}{4\pi\epsilon_0}\sum_{i=1}^{N}\sum_{j>i}^{N}\frac{e^2}{|r_i - r_j|} \tag{2.1}$$

where m_e is the electron mass, Z_i is the atomic number of the i^{th} nucleus, m_{Z_i} is the mass of i^{th} nucleus, $\hbar$ is the reduced Plancks constant, and ϵ_0 is the permittivity of vacuum.

In Eq. (2.1), the first two terms represent the kinetic energy of electrons and protons. The other terms are the various potential energies (Coulomb interactions) of nucleus-nucleus, nucleus-electron and electron-electron interactions, respectively. We can take $\mathrm{R}_i...\mathrm{R}_M$ as fixed because in reality the nuclei are much heavier than the electrons. Therefore, the first term of Eq. (2.1) will be relatively small. The nuclei-nuclei term will be effectively constant and we can redefine it as V_{II}. The wave function of the electrons will change depending on the fixed position of the nuclei. The new Hamiltonian is now simpler:

$$\hat{H} = -\sum_{i=1}^{N}\frac{h^2}{2m_e}\nabla^2_{r_i} + V_{II} - \frac{1}{4\pi\epsilon_0}\sum_{i=1}^{N}\sum_{j=1}^{M}\frac{Z_j e^2}{|r_i - R_j|} + \frac{1}{4\pi\epsilon_0}\sum_{i=1}^{N}\sum_{j>i}^{N}\frac{e^2}{|r_i - r_j|} \tag{2.2}$$

The Schrödinger equation will only depend on the position of the electrons $(r_1...r_N)$. The Schrödinger equation can be rewritten as

$$\hat{H}_e\Psi(\mathrm{r}_1...\mathrm{r}_N) = E_e\Psi(\mathrm{r}_1....\mathrm{r}_N) \tag{2.3}$$

2.1.2 Hohenberg-Kohn Theorems

Two theorems of Hohenberg and Kohn can be used to describe any many-particle system as a functional [19]. The first theorem describes the ground state particle density n and uniquely determines the external potential energy, $\mathrm{V}_{ext}(\mathrm{r})$. The main point of this theorem is that most properties of materials can be described by the particle density n. The second theorem defines the functional energy in terms of density. Thus, the minimum value of the functional will be the ground state energy and the density will be the ground state density of the system.

2.1.3 Kohn-Sham Equation

I will introduce a fictitious reference system of non-interacting particles with density ρ_s. The particles in the Kohn-Sham system are non-interacting fermions. The Kohn-Sham wave function is a single Slater determinant constructed from a set of orbitals that are the lowest energy solutions to

$$\left[-\frac{\hbar^2}{2m} + v_{eff}(r)\right]\psi_i(r) = \epsilon_i\psi_i(r) \tag{2.4}$$

Here, ϵ_i is the orbital energy of the corresponding Kohn-Sham orbital ψ_i, σ is surface density and the density for an N-particle system is

$$\rho_s(r) = \sum_{i=1}^{N}\sum_{\sigma}|\psi_i(r,\sigma)|^2 \tag{2.5}$$

The Kohn-Sham equations are named after Kohn and Sham [17].

In DFT, the total energy of a system is expressed as a functional of the charge density as

$$E(\rho) = T_s(\rho) + V_H(\rho) + V_{en} + V_{nn} + E_{xc}(\rho) \tag{2.6}$$

Adjusting the potential that these particles move under so that they have a density $\rho = \rho_s$. When N_e represents number of electron and N_n represents number of nuclei, T_s is the Kohn-Sham kinetic energy which is expressed in terms of the Kohn-Sham orbitals as

$$T_s(\rho) = -\frac{1}{2}\sum_{j=1}^{N_e} < \psi_j|\nabla_j^2|\psi_j > \tag{2.7}$$

V_H is the Hartree (or Coulomb) energy

$$V_H(\rho) = \frac{1}{2}\sum_{j=1}^{N_e}\sum_{i=1}^{N_e} < \psi_j\psi_i|\frac{1}{r_{ij}}|\psi_j\psi_i > \tag{2.8}$$

r_{ij} will never be zero because electrons have repulsive force to each other. V_{en} is electron-nuclei interaction potential energy

$$V_{en} = \sum_{a=1}^{N_n}\sum_{j=1}^{N_e} Z_a < \psi_j|\frac{1}{r_{aj}}|\psi_j > \tag{2.9}$$

V_{nn} is nuclei-nuclei interaction potential energy

$$V_{nn} = \sum_{a=1}^{N_n}\sum_{b=1}^{N_n}\frac{Z_a Z_b}{r_{ab}} \tag{2.10}$$

and $E_{xc}(\rho)$ is exchange-correlation energy. Total energy will be written as:

$$E(\rho) = -\frac{1}{2}\sum_{j=1}^{N_e} < \psi_j|\nabla_j^2|\psi_j > + \frac{1}{2}\sum_{j=1}^{N_e}\sum_{i=1}^{N_e} < \psi_j\psi_i|\frac{1}{r_{ij}}|\psi_j\psi_i > + \sum_{a=1}^{N_n}\sum_{j=1}^{N_e} Z_a < \psi_j|\frac{1}{r_{aj}}|\psi_j > + \sum_{a=1}^{N_n}\sum_{b=1}^{N_n}\frac{Z_a Z_b}{r_{ab}} + E_{xc}(\rho) \quad (2.11)$$

2.1.4 Density Functional Theory

The density can be solved by the Kohn-Sham approach which is defined in terms of Kohn-Sham orbitals [17]. The most important point is to choose a better exchange-correlation functional and basis set of orbitals. After that, from the solution of the Kohn-Sham equation, the energies, forces, and stresses can be found. There ares different methods to obtain the exchange-correlation functional. The exchange-correlation functional which defines the potential energy must be approximated except for the free electron gas. There are different types of approximations to obtain the exchange-correlation functional. The most used are the local density approximation (LDA) and the generalized gradient approximation (GGA).

2.1.4.1 Local Density Approximation

The local density approximation (LDA) (or local spin density approximation (LSDA)) says that the exchange-correlation energy is only determined by the local density, which is given by

$$\mathrm{E}_{xc}[n(r)] = \int_{\mathrm{V}} n(r)\epsilon_{xc}[n(r)]d^3r \quad (2.12)$$

where $\epsilon_{xc}[n(r)]$ is the energy which depends on the density n per electron, $\mathrm{E}_{xc}[n(r)]$ is homogeneous in the electron gas, and the integral is over the volume of the system V.

Therefore the exchange part will have an analytical form. The correlation part was calculated analytically using Monte Carlo methods in [4].

2.1.4.2 Generalized Gradient Approximation

Many modern codes using DFT now use more advanced approximations to improve accuracy for certain physical properties. The DFT calculations in this study have been made using the Generalized Gradient Approximation (GGA) [21, 30, 27]. As stated above, the LDA uses the exchange-correlation energy for the uniform electron gas at every point in the system regardless of the homogeneity of the real charge density. For nonuniform charge densities the exchange-correlation energy can deviate significantly from the uniform result. This deviation can be expressed in terms of the gradient and higher spatial derivatives of the total charge density. The GGA uses the gradient of the charge density to correct for this deviation.The generalized gradient approximation (GGA) includes the gradient of the electron density in addition to the LDA terms

$$\mathrm{E}_{xc}[n(r), \nabla n(r)] = \int n(r)\epsilon_{xc}[n(r), \nabla n(r)]d^3r \tag{2.13}$$

There are two ways to represent the gradient of functionals: Perdew-Wang (PW91) and Perdew-Burke-Ernzerhof (BE) [29, 8]. For systems where the charge density is slowly varying, the GGA has proved to be an improvement over LDA.

2.1.4.3 Pseudopotential

The electrons close to an atomic core are much less affected by surrounding atoms than are the valence electrons. Assuming the core electrons and core are fixed, a pseudopotential approach replaces the combined effects of the core electrons and Coulomb potential from the atomic core by a single pseudopotential that acts only on the valence electrons. The resulting pseudo wave-functions of the valence electrons are then smoother and the number of plane waves required to represent them is lower, resulting in faster convergence of the total energy with respect to the plane wave energy cutoff. For r longer than the cutoff radius r_c which is the radius which makes inter-atomic potential and force negligible, the full wave function and pseudo wave-function match each other. The norm conservation condition ensures that pseudo wave-functions and all electron wave functions generate the same charge densities. Ultrasoft pseudo-potentials introduced later do not impose the norm conservation constrain, providing the benefit of more smooth wave functions and smaller cutoff radii than the norm conserving pseudopotentials. A certain drawback of pseudopotentials is due to the nonlinearity of the exchange-correlation functional in DFT [11]. Elaborate nonlinear core corrections are required for an accurate description of valence-core interaction in all systems where the overlap between core and valence

electron densities is not negligible [32]. It is possible to reconstruct the complete electron density and to avoid the necessity of non-linear core corrections by using the PAW approach developed by Blöchl [3].

2.1.4.4 Basis Set

The Kohn-Sham equations can be solved by various iteration methods [24, 37]. The starting point of these iteration methods is an appropriately chosen set of basis functions. In my case, VASP uses the plane wave (PW) basis set which has two advantages. First is that it allows control of basis set convergence and second is that it enables us to calculate the forces very clearly which are acting on each atom and also unit cell stress using the Hellmann-Feynman theorem [10]. Another advantage of PW is that it helps us to understand the quantum *ab initio* molecular dynamic simulation steps.

CHAPTER 3

MAGNETIC PROPERTIES OF ZINC-TIN-SUBSTITUTED STRONTIUM HEXAFERRITE

3.1 Introduction

Strontium hexaferrite ($SrFe_{12}O_{19}$) is one of the most useful permanent magnetic materials among the various M-type hexaferrites $MFe_{12}O_{19}$ (M = Sr, Ba, or Pb) because of its chemical stability, high coercivity, saturation of magnetization, and large magneto-crystalline anisotropy [12, 5, 6, 33, 9]. High-density magnetic recording media, microwave devices and electronic wave absorbers have been getting more attention during the lasts few decades [7, 14].

M-type hexaferrite materials have a hexagonal lattice (space group $P6_3/mmc$) as shown in Fig. 3.1. In the molecule, magnetic iron ions (Fe^{3+}) have five different types of interstitial sites, including three octahedral sites ($12k$, $4f_2$, $2a$), one tetrahedral site ($4f_1$), and one trigonal bipyramid or hexahedral site ($2b$), which are shown in Table 3.1. Also, it shows Wyckoff position which is a point belonging to a set of points for which site symmetry groups are conjugate subgroups of the space group in crystallography. Total magnetization of a material is the summation of the interstitial iron sites magnetization. Iron ions which are at different sites in strontium hexaferrite help to predict the various properties of substituted strontium hexafer-

rite. For instance, Néel and Anderson proposed super-exchange interactions through oxygen ions [17, 2, 25]. Also, Gorter proposed a scheme for compounds [13]. Based on Gorters configuration of the magnetization of the five sites (iron sites), the ferric ions in the $12k$, $2a$, and $2b$ sites are anti-parallel to those of the other sites that have ferric ions in the $4f_1$ and $4f_2$ sites. The electronic structure of stoichiometric strontium hexaferrite (SrM) was calculated by Fang using the local spin density approximation in DFT [9].

In figure 3.1, blue spheres represent strontium atoms, purple spheres represent iron atoms, and red spheres represent oxygen atoms. $SrFe_{12}O_{19}$ of Gorter's form. Space group parameters are $P63/mmc$, $a = 0.58836$ nm $c = 2.30376$ nm [15].

Table 3.1

The coordinates of atoms and their symmetries in strontium hexaferrite.

Atoms	Wyckoff site	Symetry	Atom coordinates
Sr	2d	$\overline{6}m2$	$\frac{1}{3}$, $\frac{2}{3}$, $\frac{3}{4}$
Fe(1)	2a	$\overline{3}m$	0, 0, 0
Fe(2)	2b	$\overline{6}m$	0, 0, $\frac{1}{4}$
Fe(3)	4f1	$3m$	$\frac{1}{3}$, $\frac{2}{3}$, 0.02718
Fe(4)	4f2	$3m$	0.16886, 0.33772, 0.89083
Fe(5)	12k	m	0, 0, 0.1514
O(1)	4e	$3m$	0, 0, 0.9446
O(2)	4f	$3m$	0.1819, 0.3639, $\frac{1}{4}$
O(3)	6h	mm	0.1564, 0.3127, 0.05252
O(4)	12k	m	0.1564, 0.3127, 0.05252
O(5)	12k	m	0.5039, 0.0078, 0.15092

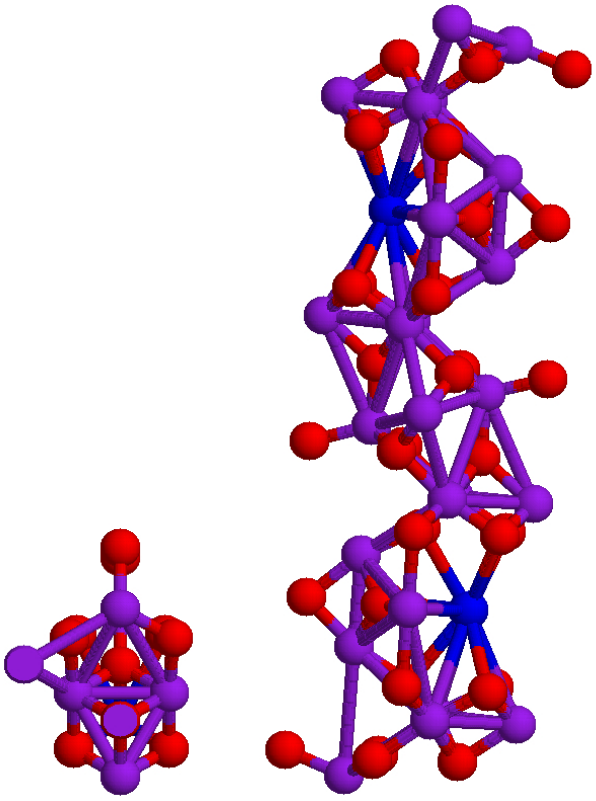

(a) From top (b) From side

Figure 3.1

The structure of strontium hexaferrite ($2SrFe_{12}O_{19}$).

Coercivity, anisotropy, and saturation magnetization are helpful properties to understand the magnetic behavior of a material. It has been found experimentally that the saturation magnetization increases with an increase of equally substituted Zn and Sn [12]. Knowledge of which sites are more preferable can enhance our understanding of saturation magnetization because each site has its special magnetic moment.

3.2 Simulation Process

For this work, each unit cell contains two formula units of strontium hexaferrite, so there are 64 atoms per unit cell, and I used periodic boundary conditions. Geometry optimizations formed the most natural structure and the energy for these structures were calculated by using Blöchl′s all-electron projector augmented wave method as implemented by Kresse and Joubert [3, 18]. I used the generalized gradient approximation (GGA) using the Perdew-Burke-Ernzerhof scheme [28]. The Vosko, Wilk and Nusair formula is used for standard interpolation for the correlation part of the exchange correlation functional [36]. After we tried various K-points, the plane-wave cut off energy was set to 520 eV for all computational processes because there is no significant change greater than 520 eV cut off energy. Geometry relaxations were done using the tetrahedron method with Blöchl′s correction and using the conjugate gradient algorithm. Geometry relaxation is calculated for 0.001 eV sensivity (Table 3.2) which means that the iterations continued until the energy differences for each successive ionic step were less than 0.001 eV. The last initial value for the

Brillouin zone, which is the set of points in k-space (49 k-points are enough) found by using the Monkhorst-Pack scheme is shown in Figure 3.2 [23]. After simulation had enough K-points, the total energy does not significantly change with increasing number of K-points.

In Table 3.2, the K-mesh is the input point sets in k-space (a×b×c). The symmetry irreducible set of k-points was determined from the crystal space group using the full Monkhorst-Pack grids [23]. The energy column helps us to decide when enough K-points have been utilized for convergence. c represents the z-direction in the K-point mesh.

3.3 Results and Conclusion

I have calculated the total energy of pure strontium hexaferrite for various spin configurations. Relaxed energy differences for different spin orientations are shown in Table 3.3 for three different K-point meshes ($5 \times 5 \times 1$, $13 \times 13 \times 1$, $14 \times 14 \times 1$) given relative to Gorter's configuration [13]. For strontium hexaferrite, Gorter configuration corresponds to + + - - + ($2a$, $2b$, $4f_1$, $4f_2$, and $12k$ respectively) spin alignment. Also, the spin alignment + + + + + corresponds to an excited spin state. The accepted value for the magnetic moment is 40 μ_B [26]. When I changed spin configuration from Gorter's configuration to the excited spin state, the magnetic moments change as shown in Table 3.3.

In the present case, we are interested in the site preference of Sn and Zn atoms if they are constrained to occupy two equivalent atomic sites. We considered only

Table 3.2

Total energy dependence on K-points for strontium hexaferrite.

K-points Mesh	Symmetry Irreducible K-points	Energy (eV)
2×2×1	2	-474.3992
3×3×1	3	-474.4185
4×4×1	6	-474.4129
5×5×1	5	-474.4145
6×6×1	12	-474.4131
7×7×1	8	-474.4133
8×8×1	20	-474.4132
9×9×1	12	-474.4134
10×10×1	30	-474.4134
11×11×1	16	-474.4136
12×12×1	42	-474.4135
13×13×1	21	-474.4134
14×14×1	56	-474.4135
15×15×1	27	-474.4135
16×16×1	72	-474.4134
17×17×1	33	-474.4134
18×18×1	90	-474.4134
19×19×1	40	-474.4133

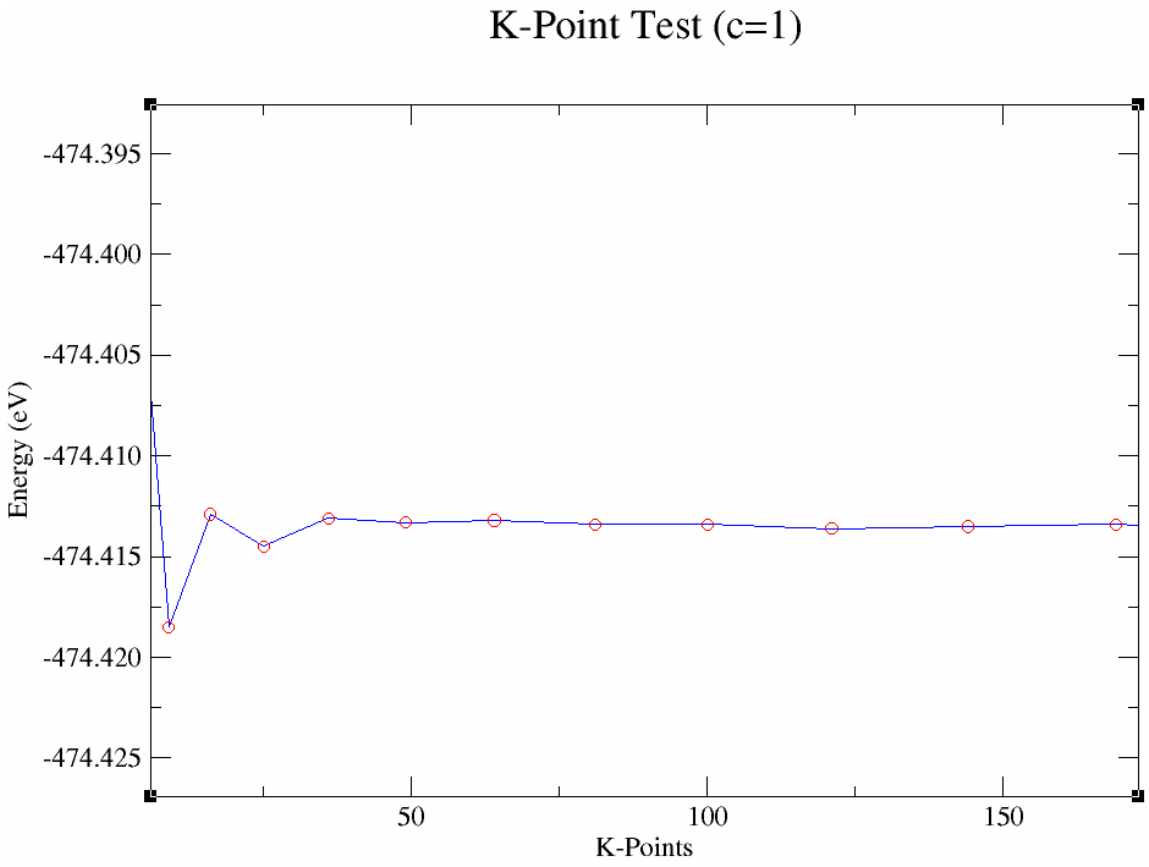

Figure 3.2

Calculated total energy as a function of the number of K-points.

the case which Sn and Zn atoms replace Fe atoms in $SrFe_{12-x}(Sn_{0.5}Zn_{0.5})_xO_{19}$ for x=1. Since the experimental results show the reduction of magnetic anisotropy, and because the anisotropy is usually attributed to the Fe atoms at $2b$ site, Ghasemi et al. suggested that Zn and Sn atoms would occupy $2b$ and $4f_2$ sites [12]. However, our DFT calculation shows that the reduction of magnetic anisotropy is possible even when Fe atoms at $4f_1$ and $4f_2$ sites are substituted by Sn and Zn atoms. In Table 3.4, the relative heats of formation (HF_rel) are small compared to the ground state energy when $2a$ site is substituted (-0.9 eV). Also, in Table 3.4, more detailed information for the magnetic moment of each atom site is shown separately. Cf column shows the site of substitution. During this substitution process, all possibilities are used. For instance, $2a$ site has two way to substitute which is Zn-Sn or Sn-Zn. The DFT model shows $4f_1$ and $4f_2$ sites are more preferable when substitution atoms (Sn and Zn) are not restricted to go to the same sites [22]. Therefore, we conclude that Sn and Zn prefer $2a$ site when both of them are constrained to occupy the same site because the system has the lowest relative heat of formation in this case. In Table 3.3 Energies are given relative to the Gorter's configuration. Plus and minus (+ and -) signs represent magnetic moments of atoms on each site.

Table 3.3

Effect of K-points and spin configuration on energy and magnetic moment.

	Spin direction of Fe ions in $SrFe_{12}O_{19}$						
Kpoints	$2a$	$2b$	$4f_1$	$4f_2$	$12k$	Energy diff. (eV/Unit cell)	Moments(μ_B/Unit cell)
25	+	+	-	-	+	0.00	39.6915
25	+	+	+	+	+	2.177	48.0001
169	+	+	-	-	+	0.00	36.6191
169	+	+	+	+	+	0.9595	32.9848
196	+	+	-	-	+	0.00	31.8810
196	+	+	+	+	+	1.92	47.9621

Table 3.4

Effect of Zn-Sn-substitution for strontium hexaferrite.

Ss[a]	Sr	O(1)	O(2)	O(3)	O(4)	O(5)	Fe(1)	Fe(2)	Fe(3)	Fe(4)	Fe(5)	σ_s [b]	$\Delta\sigma_s$ [c]	HF_rel[d]
$2a$	-0.002	-6.675	-6.299	13.804	12.393	-43.645	-1.307	0.216	0.355	-12.659	33.782	28.985	-10.491	-0.908
$2a$	-0.002	-6.677	-6.301	13.802	12.397	-43.715	-1.097	0.071	0.350	-12.604	33.732	28.991	-10.485	-0.902
$2b$	-0.001	-6.891	-6.515	13.894	12.072	-43.067	-1.122	-0.017	0.094	-10.718	33.237	29.804	-9.671	-0.411
$2b$	-0.001	-6.894	-6.518	13.890	11.929	-42.923	-1.121	-0.034	0.087	-10.824	33.385	29.832	-9.643	-0.413
$4f_1$	-0.004	-6.811	-6.648	14.216	12.336	-42.558	-0.811	0.093	-0.289	-3.559	32.813	38.459	-1.016	1.601
$4f_1$	0.000	-6.884	-6.783	14.077	12.327	-42.589	-0.817	-0.151	-0.543	-4.308	29.940	33.715	-5.760	1.614
$4f_1$	-0.003	-6.780	-6.667	14.211	12.333	-42.281	-1.102	0.054	-0.256	-3.605	32.869	38.461	-1.014	1.561
$4f_1$	-0.002	-6.808	-6.862	14.209	12.304	-42.189	-0.767	-0.098	-0.526	-1.703	30.433	37.656	-1.820	1.606
$4f_1$	-0.001	-6.789	-6.721	14.183	12.362	-42.466	-0.681	-0.151	-0.345	-3.199	32.096	37.945	-1.531	1.565
$4f_1$	-0.002	-6.771	-6.667	14.322	12.331	-41.811	-0.931	0.047	-0.263	-0.911	32.903	42.158	2.683	1.515
$4f_1$	-0.002	-6.823	-6.808	14.227	12.305	-42.230	-0.737	-0.085	-0.455	-1.413	30.321	37.970	-1.505	1.731
$4f_1$	-0.004	-6.813	-6.718	14.242	12.353	-42.588	-0.710	0.113	-0.265	-4.723	34.431	39.041	-0.435	1.728
$4f_1$	-0.003	-6.810	-6.674	14.272	12.314	-42.362	-1.086	0.070	-0.261	-3.707	32.770	38.193	-1.282	1.569
$4f_1$	-0.002	-6.870	-6.804	14.208	12.330	-41.959	-0.888	0.012	-0.558	-1.356	31.766	39.603	0.127	1.757
$4f_1$	-0.003	-6.810	-6.660	14.325	12.333	-42.088	-0.666	0.118	-0.386	-1.173	32.851	41.741	2.266	1.564
$4f_1$	0.000	-6.887	-6.688	14.084	12.298	-42.599	-0.884	-0.277	-0.527	-4.087	28.001	31.856	-7.619	1.185

[a] Ss represents substituted site

[b] σ_s is the saturation magnetization

[c] $\Delta\sigma_s$ is the σ_s relative to pure strontium hexaferrite

[d] $HF\_rel = E_{\mathrm{tot}} - 2E_{\mathrm{Sr}} - 24E_{\mathrm{Fe}} - 38E_{\mathrm{O}} + E_{\mathrm{Sn}} + E_{\mathrm{Zn}}$

Table 3.4

Effect of Zn-Sn-substitution for strontium hexaferrite. (continued)

Ss[a]	Sr	O(1)	O(2)	O(3)	O(4)	O(5)	Fe(1)	Fe(2)	Fe(3)	Fe(4)	Fe(5)	σ_s[b]	$\Delta\sigma_s$[c]	HF_rel[d]
$4f_2$	0.021	-6.903	-6.882	13.461	12.869	-43.219	-1.068	0.302	-0.041	-0.397	26.120	33.434	-6.041	0.974
$4f_2$	0.020	-6.881	-6.822	13.490	12.803	-43.355	-0.981	0.147	-0.196	-0.470	25.482	32.448	-7.028	1.737
$4f_2$	0.025	-6.953	-6.659	13.574	12.778	-43.410	-1.004	0.118	0.127	-0.104	26.788	34.509	-4.967	0.911
$4f_2$	0.024	-6.708	-6.808	13.613	12.703	-43.145	-0.944	0.369	-0.023	0.463	28.324	37.276	-2.199	1.293
$4f_2$	0.024	-6.819	-6.870	13.530	12.624	-43.231	-1.068	0.263	-0.392	-1.560	27.524	33.092	-6.383	1.054
$4f_2$	0.024	-6.941	-6.630	13.564	12.678	-43.375	-0.990	0.243	0.093	0.160	25.826	33.840	-5.635	1.303
$4f_2$	0.016	-6.844	-6.801	13.572	12.722	-43.164	-0.998	0.200	-0.157	1.699	26.737	36.426	-3.049	1.287
$4f_2$	0.017	-6.780	-6.742	13.715	12.640	-42.870	-1.080	0.473	-0.122	2.987	28.637	40.286	0.810	0.647
$4f_2$	0.015	-7.045	-6.630	13.593	12.727	-43.283	-1.006	0.104	0.049	2.053	24.276	33.853	-5.623	1.008
$4f_2$	0.024	-6.768	-6.918	13.505	12.773	-43.339	-0.938	0.256	-0.247	-2.427	27.403	32.431	-7.044	0.725
$4f_2$	0.021	-6.820	-6.958	13.450	12.868	-43.179	-1.130	0.441	-0.129	-2.499	28.281	33.518	-5.957	0.975
$4f_2$	0.020	-6.986	-6.720	13.489	12.746	-43.477	-1.070	0.133	-0.201	-0.733	24.065	30.153	-9.322	1.372

[a] Ss represents substituted site

[b] σ_s is the saturation magnetization

[c] $\Delta\sigma_s$ is the σ_s relative to pure strontium hexaferrite

[d] $HF\_rel = E_{\text{tot}} - 2E_{\text{Sr}} - 24E_{\text{Fe}} - 38E_{\text{O}} + E_{\text{Sn}} + E_{\text{Zn}}$

REFERENCES

[1] S. Alamolhoda, S. S. Ebrahimi, and A. Badiei, "A study on the formation of strontium hexaferrite nanopowder by a sol-gel auto-combustion method in the presence of surfactant," *Journal of Magnetism and Magnetic Materials*, vol. 303, no. 1, 2006, pp. 69 – 72.

[2] P. W. Anderson, "Antiferromagnetism. Theory of Superexchange Interaction," *Phys. Rev.*, vol. 79, no. 2, Jul 1950, pp. 350–356.

[3] P. E. Blöchl, "Projector augmented-wave method," *Phys. Rev. B*, vol. 50, no. 24, Dec 1994, pp. 17953–17979.

[4] D. M. Ceperley and B. J. Alder, "Ground State of the Electron Gas by a Stochastic Method," *Phys. Rev. Lett.*, vol. 45, no. 7, Aug 1980, pp. 566–569.

[5] D. H. Choi, S. Y. An, S. W. Lee, I.-B. Shim, and C. S. Kim, "Site occupancy and anisotropy distribution of Al substituted Ba-ferrite with high coercivity," *physica status solidi (b)*, vol. 241, no. 7, 2004, pp. 1736–1739.

[6] M. C. Dimri, S. C. Kashyap, and D. C. Dube, "Electrical and magnetic properties of barium hexaferrite nanoparticles prepared by citrate precursor method," *Ceramics International*, vol. 30, no. 7, 2004, pp. 1623 – 1626, 3rd Asian Meeting on Electroceramics.

[7] N. Dishovski, A. Petkov, I. Nedkov, and I. Razkazov, "Hexaferrite contribution to microwave absorbers characteristics," *Magnetics, IEEE Transactions on*, vol. 30, no. 2, mar 1994, pp. 969 –971.

[8] M. Ernzerhof and G. E. Scuseria, "Assessment of the Perdew–Burke–Ernzerhof exchange-correlation functional," *The Journal of Chemical Physics*, vol. 110, no. 11, 1999, pp. 5029–5036.

[9] C. M. Fang, F. Kools, R. Metselaar, G. de With, and R. A. de Groot, "Magnetic and electronic properties of strontium hexaferrite $SrFe_{12}O_{19}$ from first-principles calculations," *Journal of Physics Condensed Matter*, vol. 15, Sept. 2003, pp. 6229–6237.

[10] R. P. Feynman, "Forces in Molecules," *Phys. Rev.*, vol. 56, no. 4, Aug 1939, pp. 340–343.

[11] W. M. C. Foulkes and R. Haydock, "Tight-binding models and density-functional theory," *Phys. Rev. B*, vol. 39, no. 17, Jun 1989, pp. 12520–12536.

[12] A. Ghasemi, V. Sepelak, X. Liu, and A. Morisako, "The role of cations distribution on magnetic and reflection loss properties of ferrimagnetic $SrFe_{12-x}(Sn_{0.5}Zn_{0.5})_xO_{19}$," *Journal of Applied Physics*, vol. 107, no. 9, 2010, p. 09A734.

[13] E. Gorter, "Saturation magnetization of some ferrimagnetic oxides with hexagonal crystal structures," *Proceedings of the IEE - Part B: Radio and Electronic Engineering*, vol. 104, no. 5, 1957, pp. 255 –260.

[14] S. E. Jacobo, L. Civale, and M. A. Blesa, "Evolution of the magnetic properties during the thermal treatment of barium hexaferrite precursors obtained by coprecipitation from barium ferrate (VI) solutions," *Journal of Magnetism and Magnetic Materials*, vol. 260, Mar. 2003, pp. 37–41.

[15] K. Kimura, M. Ohgaki, K. Tanaka, H. Morikawa, and F. Marumo, "Study of the bipyramidal site in magnetoplumbite-like compounds, SrM12O19 (M = Al, Fe, Ga)," *Journal of Solid State Chemistry*, vol. 87, no. 1, 1990, pp. 186 – 194.

[16] W. Kohn, A. D. Becke, and R. G. Parr, "Density Functional Theory of Electronic Structure," *The Journal of Physical Chemistry*, vol. 100, no. 31, 1996, pp. 12974–12980.

[17] W. Kohn and L. J. Sham, "Self-Consistent Equations Including Exchange and Correlation Effects," *Phys. Rev.*, vol. 140, no. 4A, Nov 1965, pp. A1133–A1138.

[18] G. Kresse and D. Joubert, "From ultrasoft pseudopotentials to the projector augmented-wave method," *Phys. Rev. B*, vol. 59, no. 3, Jan 1999, pp. 1758–1775.

[19] E. S. Kryachko, "Hohenberg-Kohn theorem," *International Journal of Quantum Chemistry*, vol. 18, no. 4, 1980, pp. 1029–1035.

[20] K. Laasonen, R. Car, C. Lee, and D. Vanderbilt, "Implementation of ultrasoft pseudopotentials in ab initio molecular dynamics," *Phys. Rev. B*, vol. 43, no. 8, Mar 1991, pp. 6796–6799.

[21] D. C. Langreth and M. J. Mehl, "Beyond the local-density approximation in calculations of ground-state electronic properties," *Phys. Rev. B*, vol. 28, no. 4, Aug 1983, pp. 1809–1834.

[22] L. S. Liyanage, "private communication," Mississippi State University, 2011.

[23] H. J. Monkhorst and J. D. Pack, "Special points for Brillouin-zone integrations," *prb*, vol. 13, jun 1976, pp. 5188–5192.

[24] R. C. Morrison and Q. Zhao, "Solution to the Kohn-Sham equations using reference densities from accurate, correlated wave functions for the neutral atoms helium through argon," *Phys. Rev. A*, vol. 51, no. 3, Mar 1995, pp. 1980–1984.

[25] L. Néel, "Magnetic properties of ferrites: Ferromagnetism and antiferromagnetism," *Phys. Rev.*, vol. 79, no. 2, Jul 1950, pp. 350–356, *Orginal article was French*.

[26] P. Novák and J. Rusz, "Exchange interactions in barium hexaferrite," *Phys. Rev. B*, vol. 71, no. 18, May 2005, p. 184433.

[27] J. P. Perdew, "Density-functional approximation for the correlation energy of the inhomogeneous electron gas," *Phys. Rev. B*, vol. 33, no. 12, Jun 1986, pp. 8822–8824.

[28] J. P. Perdew, K. Burke, and M. Ernzerhof, "Generalized Gradient Approximation Made Simple," *Phys. Rev. Lett.*, vol. 77, no. 18, Oct 1996, pp. 3865–3868.

[29] J. P. Perdew and Y. Wang, "Accurate and simple analytic representation of the electron-gas correlation energy," *Phys. Rev. B*, vol. 45, no. 23, Jun 1992, pp. 13244–13249.

[30] J. P. Perdew and W. Yue, "Accurate and simple density functional for the electronic exchange energy: Generalized gradient approximation," *Phys. Rev. B*, vol. 33, no. 12, Jun 1986, pp. 8800–8802.

[31] S. Picozzi, A. Continenza, and A. J. Freeman, "$Co2MnX$ ($X = Si$, Ge, Sn) Heusler compounds: An ab initio study of their structural, electronic, and magnetic properties at zero and elevated pressure," *Phys. Rev. B*, vol. 66, no. 9, Sep 2002, p. 094421.

[32] E. L. Shirley, R. M. Martin, G. B. Bachelet, and D. M. Ceperley, "Role of forms of exchange and correlation used in generating pseudopotentials," *Phys. Rev. B*, vol. 42, no. 8, Sep 1990, pp. 5057–5066.

[33] D. Sriram, R. L. Snyder, and V. R. W. Amarakoon, "Anisotropic thermal expansion of barium hexaferrite using dynamic high-temperature x-ray diffraction," *Journal of Materials Research*, vol. 15, June 2000, pp. 1349–12353.

[34] C. Surig, K. A. Hempel, and D. Bonnenberg, "Formation and microwave absorption of barium and strontium ferrite prepared by sol x2010;gel technique," *Applied Physics Letters*, vol. 63, no. 20, nov 1993, pp. 2836 –2838.

[35] Y. Umeno, Y. Kinoshita, and T. Kitamura, "Ab initio DFT simulation of ideal shear deformation of SiC polytypes," *Modelling Simul. Mater. Sci. Eng.*, vol. 15, Mar. 2007, pp. 27–37.

[36] S. H. Vosko and L. Wilk, "Influence of an improved local-spin-density correlation-energy functional on the cohesive energy of alkali metals," *Phys. Rev. B*, vol. 22, no. 8, Oct 1980, pp. 3812–3815.

[37] J. Wang and T. L. Beck, "Efficient real-space solution of the Kohn–Sham equations with multiscale techniques," *The Journal of Chemical Physics*, vol. 112, no. 21, 2000, pp. 9223–9228.

[38] Y. Wang and J. P. Perdew, "Spin scaling of the electron-gas correlation energy in the high-density limit," *Phys. Rev. B*, vol. 43, no. 11, Apr 1991, pp. 8911–8916.